Int. J. Vehicle Design, Vol.

Knock limit prediction via multi-zone modelling of a Primary Reference Fuel HCCI engine

Tommy Tzanetakis, Priyanka Singh, Ju-Tsung Chen and Murray J. Thomson*

Department of Mechanical and Industrial Engineering,
University of Toronto,
5 King's College Road,
Toronto ON, M5S 3G8, Canada
E-mail: tzaneta@mie.utoronto.ca
E-mail: priyanka.singh@utoronto.ca
E-mail: jutsung.chen@utoronto.ca
E-mail: thomson@mie.utoronto.ca
*Corresponding author

Charles R. Koch

Department of Mechanical Engineering,
University of Alberta,
4-9 Mechanical Engineering Building,
Edmonton AB, T6G 2G8, Canada
E-mail: bob.koch@ualberta.ca

Abstract: A multi-zone model was used to predict the combustion behaviour of a single cylinder Homogeneous Charge Compression Ignition (HCCI) engine. Blow-by was considered to capture engine performance at the low operating speed of 700 rpm. The model was calibrated and verified by matching predicted and experimental pressure traces at two engine operating points. The calculated CO and Unburned Hydrocarbon (UHC) emissions showed good agreement with experiments at both points. The onset of knock during HCCI was adequately reproduced using the Maximum Pressure Rise Rate (MPRR) criterion and another method based on the pressure equalisation rate within the charge.

Keywords: internal combustion engine; HCCI; homogeneous charge compression ignition; PRFs; primary reference fuels; excess air dilution; EGR; exhaust gas recirculation; multi-zone modelling; blow-by; MPRR; maximum pressure rise rate; UHCs; unburned hydrocarbons; knock boundary prediction.

Reference to this paper should be made as follows: Tzanetakis, T., Singh, P., Chen, J-T., Thomson, M.J. and Koch, C.R. (2010) 'Knock limit prediction via multi-zone modelling of a Primary Reference Fuel HCCI engine', *Int. J. Vehicle Design*, Vol.

Biographical notes: Tommy Tzanetakis received his BASc and MASc in Mechanical Engineering from the University of Toronto, Canada, in 2004 and 2006, respectively. He is currently a PhD candidate in the same department. His research deals with characterising the spray combustion behaviour of cellulose derived biofuels for use in potential combined heat and power applications.

Priyanka Singh received her BASc in Mechanical Engineering from the University of Toronto, Canada, in 2009. During her professional experience year between 2007 and 2008, she was an intern in the Mechanical Maintenance Support Department at CAMI Automotive Inc., Ingersoll, Ontario, Canada. Since September of 2009 she has been working as a Dimensional Integrity Group Specialist at the same company.

Ju-Tsung Chen received his BASc in Mechanical Engineering from National Taiwan University, Taipei, Taiwan, in 1989, and his MEng at the University of Toronto, Canada, in 2007. From 1991 to 1996, he worked for the Nissan Motor Company in Sanyi, Taiwan, modelling and designing automobile parts. In 1991, he joined First International Computer Inc. in Taipei, Taiwan as a Technical Support Engineer. From 1997 to 2005, he worked as a Technical Support Manager at Alpha Precision Instrumentation Company, Taipei, Taiwan. Since 2008 he has been working for Algonquin Automotive Inc., Huntsville, Ontario, Canada, where he models and designs automobile components.

Murray J. Thomson received his BEng. in Mechanical Engineering from McGill University, Montreal, Canada, in 1986, and his MSc and PhD from the University of California, Berkeley, CA, in 1992 and 1994, respectively. From 1994 to 1996, he worked for Goodfellow Consultants, Inc. in Toronto, Canada. In 1996, he joined the Mechanical and Industrial Engineering Department of the University of Toronto, where he is a Professor. His research interests include combustion, air pollution and biofuels.

Charles R. Koch received his BSc in Mechanical Engineering from the University of Alberta, Edmonton, Canada in 1985, and his MSc and PhD from Stanford University, Palo Alto, CA, in 1986 and 1991, respectively. From 1991 to 1992 and from 1994 to 2001 he worked for Daimler-Benz in Stuttgart, Germany, in advanced internal combustion engines. During 1992 to 1994, he worked for General Motors. In 2001, he joined the Mechanical Engineering Department of the University of Alberta, Edmonton Canada, where he is a Professor. His research interests include combustion engines, advanced powertrains and control of fluid systems.

1 Introduction

1.1 Combustion characteristics

Homogeneous Charge Compression Ignition (HCCI) may be considered as a hybrid between conventional Spark Ignition (SI) and Compression Ignition (CI) combustion modes. In HCCI engines, a premixed charge of fuel and air is introduced into the cylinder and compressed to the point of auto-ignition. Visual studies by Onishi et al. (1979) have shown that much of the mixture ignites and burns simultaneously without the

development of a propagating flame front. HCCI combustion is therefore primarily limited by the chemical kinetic timescales of auto-ignition. The work by Christensen and Johansson (2002) confirmed this by demonstrating that the direct effect of in-cylinder turbulence on HCCI combustion is relatively minor. Rapid combustion of this type means that HCCI engines approach the ideal constant volume cycle and exhibit relatively high rates of heat release compared to SI and CI combustion. When combined with wide open throttle operation and the high compression ratios that are needed to achieve ignition, HCCI engines can reach near diesel thermal efficiencies (Thring, 1989; Christensen et al., 1997). The high rates of heat release observed in HCCI mean that a great deal of dilution in the form of excess air or Exhaust Gas Recirculation (EGR) is required to limit the occurrence of knock (Thring, 1989). In fact, the knock exhibited in HCCI engines imposes a formidable restriction on high load operation. As a result, naturally aspirated HCCI engines are typically limited to part-load operation with a typical Indicated Mean Effective Pressure (IMEP) between 1 to 5 bar (Christensen et al., 1997). Advantages of HCCI combustion include simultaneous near zero NO_x and soot emissions since the charge is typically lean and well mixed (Suzuki et al., 1997). However, the low peak cylinder temperatures which help to limit NO_x formation can also result in incomplete combustion and localised quenching which are responsible for relatively high UHC and CO emissions (Christensen et al., 1997).

1.2 Dilution control strategies and high load (knock) limit

One of the most important practical issues related to implementing HCCI is the development of effective combustion control strategies. Since HCCI relies on chemical auto-ignition, there is no direct way (in-cylinder spark or fuel injection) of controlling ignition timing or the rate of heat release. Therefore, indirect techniques such as changing the air/fuel ratio must be utilised (Milovanovic and Chen, 2001). Perhaps the simplest and most practically realisable control strategies are excess air and EGR charge dilution. Increasing the amount of excess air within a charge displaces fuel and reduces the total energy that can be released. This results in lower peak temperatures and pressures as well as a reduced rate of heat release. In a similar fashion, increasing the EGR rate also reduces peak temperature and pressure while extending the burn duration (Milovanovic and Chen, 2001).

Several previous experimental studies (Thring, 1989; Oakley et al., 2001a, 2001b; Atkins and Koch, 2005; Kalghatgi and Head, 2005; Yoshizawa et al., 2006; Yao et al., 2007) have investigated this control strategy and plotted the HCCI operating region for various fuels including gasoline, methanol, ethanol and a complete range of Primary Reference Fuel (PRF) mixtures. One of the most important features of the operating maps that were generated is the high load limit which occurs at relatively low dilution rates. In all the cases investigated this limit was reached when

i the pressure rise rate in the cylinder exceeded a certain threshold value

ii acoustic pressure wave oscillations that developed within the combustion chamber had a frequency that corresponded to a characteristic chamber resonant frequency

iii the amplitude of these oscillations exceeded a threshold value, or

iv the audible noise or ‘knock’ that was generated by these oscillations exceeded a certain threshold.

Results from these studies indicate that all of the above methods are adequate for consistently determining the high load limit of HCCI engines and that they are indeed correlated to one another. However, these criteria were simply extended from conventional SI knock detection strategies without developing a fundamental understanding of the knock phenomenon specific to HCCI.

1.3 HCCI and knock

In SI engines, knock occurs when end gas is forced to auto-ignite before it is reached by a turbulent, propagating flame front. As stated in Yelvington and Green (2003), it is the competition between turbulent flame speed and ignition delay which ultimately determines if knock occurs in this situation. In HCCI combustion there is no propagating flame front, therefore Yelvington and Green (2003) argue that knock is more closely related to the development of localised overpressures within the charge. Using this concept they proposed that if a portion of gas exhibits a rate of heat release which exceeds its maximum rate of expansion, then that portion of gas is likely to experience a localised overpressure (Yelvington and Green, 2003; Yelvington et al., 2004). The maximum rate of expansion for any portion of gas would be governed by the speed of sound. It is clear that the presence of sustained pressure disparities within the cylinder would inevitably lead to the formation and propagation of the acoustic waves responsible for knock. Conversely, if all the parcels of gas within the mixture can accommodate the rate of heat release by expanding to keep the cylinder pressure uniform, the potential of forming localised pressure disparities and the onset of knock disappears. This physical model is also consistent with the experimental study of Griffiths et al. (2002) which demonstrated that knocking reactions in a homogeneous charge Rapid Compression Machine (RCM) originate from localised differences in the rates of chemical heat release. The reaction zones eventually cause a rapid acceleration in the rate of pressure rise followed by the development of acoustic oscillations within the cylinder. Based on these arguments, Yelvington and Green (2003) performed a scaling analysis on the first law of thermodynamics to derive a dimensionless parameter (β_k) which represents the ratio between the Heat Release Rate (HRR) and the expansion rate for pressure equalisation in a parcel of gas:

$$\beta_k = \frac{L_c(\gamma-1)\dot{q}}{\gamma P u_{\text{sound}}}. \tag{1}$$

In this equation L_c is a characteristic length scale, γ is the ratio of specific heats for the gas, $\dot{q}$ is the rate of chemical heat release per unit volume, P is the cylinder pressure and u_{sound} is the speed of sound. When β_k exceeds a value of 1, the pressure equalisation process within the cylinder breaks down and the potential for localised overpressure and knock is realised (Yelvington and Green, 2003).

Since most HCCI models lack the ability to predict the onset of pressure wave oscillations, many studies have traditionally used a criterion based on the Maximum Pressure Rise Rate (MPRR) in order to calculate the knock boundary of HCCI engine operating regions (Yoshizawa et al., 2006). Predictions made using this technique are typically quite good since the occurrence of HCCI knock is directly related to excessive pressure rise rates. As demonstrated in Yoshizawa et al. (2006) however, this particular criterion is sensitive to specific operating conditions such as engine speed.

The β_k criterion presented in Yelvington and Green (2003) solves this problem since it was developed from basic thermodynamic principles and an understanding of the physical knock process in HCCI. As a result, this criterion is universally applicable and does not need to be calibrated for a specific engine operating condition. The use of β_k has already been implemented to predict the high load limit of HCCI engines with different operating conditions and fuels (Yelvington and Green, 2003; Yelvington et al., 2004). The overall purpose of the current work is to make a comparison between the predictive capability of the β_k and MPRR criteria in terms of calculating the knock boundary of an HCCI engine.

1.4 Prior numerical HCCI studies

Several numerical models of varying detail have been developed in order to describe HCCI combustion. Single zone models consider the in-cylinder charge as a closed, homogeneous reactor that can undergo volume change. Various studies including Flowers et al. (2000) have shown that such models can predict ignition timing and NO_x emissions trends reasonably well. Unfortunately, they tend to over-predict peak temperatures, peak pressures, the overall rate of heat release and associated performance parameters such as IMEP and thermal efficiency. The determination of these quantities should be based on a more accurate description of the mixture and temperature stratification within the charge as well as the dynamic boundary layer and crevice volume effects that occur throughout the closed engine cycle. Multi-zone models can capture these effects by considering the engine charge as a combination of several individually homogenous zones which can be distributed into boundary layers or crevice regions. Several studies have demonstrated that multi-zone models can more accurately predict overall pressure trace behaviour (Aceves et al., 2001). Finally, the most advanced models for HCCI include a full Computational Fluid Dynamics (CFD) treatment of convection, diffusion and heat transfer processes at a fairly detailed grid level and a multi-zone treatment of the actual chemical kinetic processes of combustion. The models described in Aceves et al. (2001) and Yelvington and Green (2003) use CFD to determine a mass-temperature profile for the charge just prior to combustion. Next, this profile is used to construct several coarser mass-temperature bins corresponding to a multi-zone model for subsequent calculation of heat release. Other models like the one developed in Babajimopoulos et al. (2005) incorporate a continual mapping between detailed grid CFD and multi-zone chemical kinetic calculations at every time step.

A multi-zone methodology devoid of any detailed CFD was chosen for the current work. Although they are more complicated than single zone models, multi-zone models are able to capture the overall pressure trace behaviour exhibited by HCCI engines reasonably well. Furthermore, these models are less computationally expensive than other models that are coupled to CFD codes.

It is interesting to note that the work in Yelvington et al. (2004) was essentially done using a single zone model, but the operating maps they generated were not directly compared with experimental engine maps. The prior study (Yelvington and Green, 2003) did validate multi-zone predictions of the knock boundary against the experimental work of Oakley et al. (2001a, 2001b), but did not directly demonstrate the robustness of their multi-zone model at multiple operating points via direct pressure trace comparison. The current investigation addresses these issues by thoroughly validating individual multi-zone pressure traces with experimental data at multiple operating points and using

the same model to reproduce the experimentally determined knock boundary of an HCCI engine. Furthermore, a simple blow-by model has been incorporated into the current multi-zone methodology. Several prior studies (Oakley et al., 2001a, 2001b; Yelvington and Green, 2003; Yelvington et al., 2004; Kalghatgi and Head, 2005; Yoshizawa et al., 2006; Yao et al., 2007) considered various engine speeds between 1000 rpm to 4000 rpm while the current work investigates HCCI combustion at 700 rpm, an engine speed that is low enough for blow-by to have a prominent effect.

2 Experimental data set

The experimental data modelled in this study was acquired from Atkins and Koch (2005). A single cylinder, 4-stroke Cooperative Fuels Research (CFR) engine was used to generate full cycle in-cylinder pressure traces at operating points of varying charge dilution. The operating region data for PRF20 (20% iso-octane and 80% *n*-heptane by volume) is organised in terms of an excess air ratio (λ) vs. EGR rate dilution map, as shown in Figure 1. This particular octane number fuel has not been considered in the previous knock prediction work of Yelvington and Green (2003) or Yelvington et al. (2004). λ is defined as the actual mass based air-to-fuel ratio divided by the stoichiometric mass based air-to-fuel ratio (for a given fuel); it applies only to the freshly inducted fuel-air portion of the charge and does not include air content from recycled exhaust gases. EGR rate is defined as the percent of total inducted mass that is composed of recycled exhaust gases. The lower boundary represents the high load or knock limit of the engine. This limit was evaluated using the r.m.s band-pass method which isolates the amplitude of pressure oscillations observed in the cylinder that occur at the characteristic knock frequency of the engine (Atkins and Koch, 2005). During the actual tests, this method was correlated to the audible knock generated by the engine.

Figure 1 Dilution operating map for PRF20

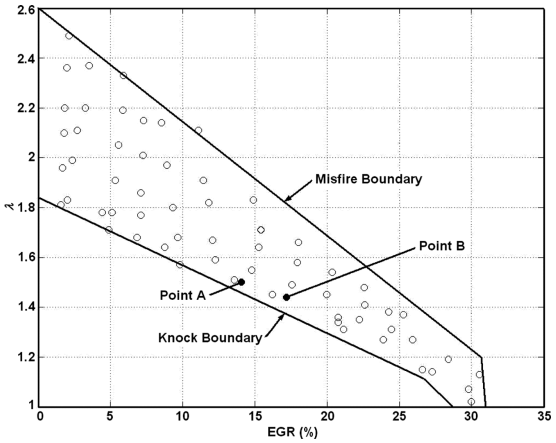

Source: Atkins and Koch (2005)

Every operating point from the experimental study is completely specified by λ and the EGR rate. Engine parameters such as compression ratio, intake temperature and even engine speed were kept as constant as possible in order to isolate the effects of dilution on

HCCI combustion. Table 1 summarises all of the relevant engine operating conditions. More specific details about the experimental apparatus as well as the data acquisition systems and processes employed may be found in Atkins and Koch (2005).

Table 1 CFR engine operating parameters

Fuel	PRF20
Compression Ratio (CR)	12 : 1
Connecting rod – Crank arm ratio (R_l)	4.44
Displacement volume	0.612 L
Bore	8.255 cm
Stroke	11.43 cm
Engine speed (ω)	700 rpm
Throttle position	Wide Open
Coolant temperature	369 K (96ºC)
Intake temperature	361 K (88ºC)
Intake valve opening	10 deg ATDC
Intake valve closing	34 deg ABDC
Exhaust valve opening	40 deg BBDC
Exhaust valve closing	15 deg ATDC

3 Numerical methodology

3.1 Zone allocation

In this study, a 10-zone model based on the work of Aceves et al. (2001) and Tzanetakis (2006) was developed. The zones are represented by a series of homogeneous reactors that are physically allocated as concentric cylindrical shells of gas within the cylinder. For simplicity, crevice regions have been lumped together with the outermost zone. Zones that successively approach combustion chamber surfaces are assigned a thickness based on the geometric model parameter R. This parameter represents how much thinner each zone successively closer to cylinder surfaces becomes as a percent of the previous zone's thickness. However, if $R = 1$, then every zone (excluding the core zone) has the same thickness. Figure 2 shows this allocation scheme when $R = 1$.

Figure 2 Representative allocation of zones within charge for $R = 1$

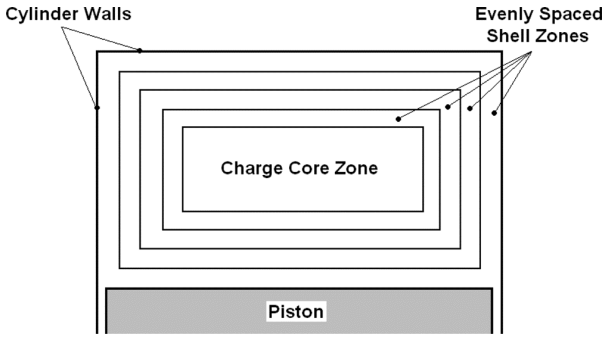

3.2 Multi-zone algorithm

Figure 3 demonstrates the overall numerical algorithm that has been adopted. The simulation occurs for the closed part of the engine cycle between Intake Valve Closure (IVC) and Exhaust Valve Opening (EVO) since knock will only occur during this interval. The blocks within the feedback loop represent calculations that are repeated for every time step.

Figure 3 Multi-zone algorithm flow diagram

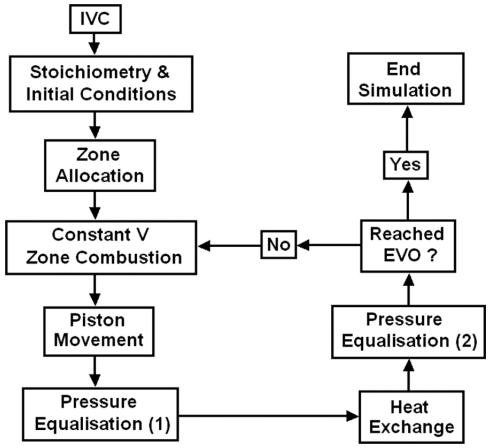

First, each zone is treated as an independent, homogeneous, constant volume reactor. There is no diffusion, mixing, heat transfer, volume change or even mass transfer between zones during this process. Given these conditions, the energy and species conservation equations at constant volume are solved simultaneously for each zone (Kee et al., 2000):

$$\frac{\mathrm{d}T}{\mathrm{d}t} = -\frac{1}{\rho c_v}\sum_{j=1}^{K} u_j \dot{\omega}_j MW_j \tag{2}$$

$$\frac{\mathrm{d}Y_j}{\mathrm{d}t} = \frac{\dot{\omega}_j MW_j}{\rho}. \tag{3}$$

Thermodynamic properties and chemical reaction rates are calculated using the CHEMKIN gas phase kinetics subroutine library (Kee et al., 2003) in combination with a reduced PRF chemical kinetic mechanism (Tanaka et al., 2003) which consists of 32 species and 55 reactions. This is different than the treatment given by Yelvington and Green (2003) and Yelvington et al. (2004) which both use a very detailed mechanism with 1034 species and 4238 reactions. Equations (2) and (3) form a set of $K + 1$ ordinary differential equations that are solved simultaneously using an iterative numerical approach. Since zones remain independent throughout this process, they develop their own pressures which are calculated using the ideal gas law (Kee et al., 2000):

$$P = \frac{\rho R_u T}{MW_{\mathrm{mix}}}. \tag{4}$$

At this point, the temperature, pressure and species concentrations for each zone are completely specified. While zones are undergoing chemical reaction however, there is also movement of the piston. The geometric relationship between total instantaneous combustion chamber volume (V_{total}) and crankshaft rotation angle (θ) from Heywood (1988) is used to calculate piston motion.

Next, the combined effect of chemical heat release and piston movement on the thermodynamic state of each zone must be calculated. This is accomplished by equalising the pressure of every zone into a single uniform cylinder pressure (P_{cyl}). The inherent assumption here is that pressure within the cylinder equalises very quickly, or more precisely, that pressure equalisation (which occurs at the speed of sound) is much faster than the influence of piston movement or the rate of chemical heat release on cylinder pressure during a given time step. This assumption means that no significant pressure gradients develop within the engine charge and is only valid when $\beta_k < 1$ for every zone at a given instant. To perform the calculation, boundary work interactions between expanding and contracting zones as well as mass loss due to engine blow-by are considered. The 1st law of thermodynamics, ideal gas law, mass conservation and volume constraint equations are written for the entire system of (i) zones (Aceves et al., 2001; Ferguson, 1986):

$$m_i c_{v,i} \mathrm{d}T_i + c_{v,i} T_i \mathrm{d}m_i + P_{\text{cyl}} \mathrm{d}V_i + m_{\text{out},i} c_{p,i} T_i = 0 \tag{5}$$

$$P_{\text{cyl}} V_i = m_i R_i T_i \tag{6}$$

$$\mathrm{d}m_i = -\frac{C_{BB} m_i}{\omega} \mathrm{d}\theta \tag{7}$$

$$\sum V_i = V_{\text{total}}. \tag{8}$$

The $P_{\text{cyl}}\mathrm{d}V_i$ term in equation (5) describes the expansion and contraction of zones while the $m_{\text{out},i}c_{p,i}T_i$ term accounts for the loss of enthalpy due to blow-by. The remaining terms represent changes in internal energy. Equation (7) is related to the blow-by model (which is discussed in the next section) while equation (8) states that the sum of zone volumes must be equal to the total cylinder volume at any given time.

Equations (5)–(8) form a set of $3i + 1$ equations with the same number of unknowns: (i) zone temperatures, (i) zone volumes, (i) zone masses and a single uniform cylinder pressure. The equations are discretised over the given time step (for instance, $\mathrm{d}T = \Delta T = T - T^o$) and solved explicitly for all the new pressure equalised quantities:

$$P_{\text{cyl}} = \frac{\sum_{i=1}^{N_{\text{zones}}} m_i^o c_{v,i}^o T_i^o \beta \left(\dfrac{1}{\gamma_i^o - 1} - \dfrac{1}{\beta} \right)^{-1}}{V_{\text{total}} - \sum_{i=1}^{N_{\text{zones}}} V_i^o \left(\dfrac{1}{\gamma_i^o - 1} - \dfrac{1}{\beta} \right)^{-1}} \tag{9}$$

$$V_i = \left[\frac{m_i^o c_{v,i}^o T_i^o \beta + P_{\text{cyl}} V_i^o}{P_{\text{cyl}}} \right] \left(\frac{1}{\gamma_i^o - 1} - \frac{1}{\beta} \right)^{-1} \tag{10}$$

$$T_i = \frac{P_{\text{cyl}} V_i}{m_i^o R_i^o \beta} \tag{11}$$

$$m_i = m_i^o \beta \tag{12}$$

$$\beta = 1 - C_{BB}\left(\frac{\Delta\theta}{\omega}\right). \tag{13}$$

Variables with a superscript 'o' refer to values calculated after independent constant volume zone combustion (just prior to pressure equalisation). The ratio of specific heats (γ) was used to present the equations in a more compact form as in Aceves et al. (2001). The parameter β is constant for a given engine operating speed (ω) and crank angle discretisation ($\Delta\theta$) and is related to the amount of blow-by experienced by each zone (not to be confused with β_k).

After pressure has been equalised, a Woschni correlation specifically adapted for HCCI engines and based on the uniform cylinder pressure is used to calculate a heat transfer coefficient (Chang et al., 2004). This coefficient is used to calculate the heat exchange between adjacent zones as well as between the outermost zone and in-cylinder surfaces. The same heat transfer coefficient is distributed to every zone boundary since turbulence is relatively even throughout the combustion chamber; CFR engines are designed to minimise the effects of turbulence (as well as its associated gradients) and promote ignition.

Once all heat transfer calculations are made, another pressure equalisation calculation is carried out in order to specify the final thermodynamic state of each zone at the end of the time step. Blow-by is not considered during this particular equalisation process. Another explicit set of expressions for final zone temperatures, volumes and equalised cylinder pressure can be formulated. These equations are identical to those developed in Tzanetakis (2006). At this point in the simulation, the conditions associated with each zone are fed back to the beginning of the algorithm as initial conditions for the next time step.

3.3 Blow-by model

The blow-by model developed in this study was derived directly from first principles. Mass continuity states that the rate of change of mass within the charge must be equal to the blow-by rate (Ferguson, 1986):

$$\frac{\mathrm{d}m}{\mathrm{d}\theta} = -\frac{\dot{m}_{BB}}{\omega}. \tag{14}$$

Since there is no mass transfer between zones, a very simple form of the blow-by rate had to be adopted. It was assumed that blow-by rate is directly proportional to the instantaneous mass within the charge (Ferguson, 1986):

$$\dot{m}_{BB} = C_{BB} m. \tag{15}$$

In this simple treatment, the constant of proportionality or blow-by constant (C_{BB}) accounts for bore shape and piston ring pack design, as well as engine load and lubrication conditions; all the major parameters that influence blow-by from one engine

operating condition to another (Ferguson, 1986; Ma et al., 1996; Cheng et al., 2004). Perhaps a more detailed blow-by model based on the instantaneous in-cylinder pressure could have been considered, but the overall effect is difficult to quantify since higher pressures not only improve the driving force for blow-by, but help to seal the ring pack as well. Therefore, the treatment given here was deemed an adequate first approximation for incorporating the overall effect of blow-by on engine performance.

Combining equations (14) and (15) leads to equation (7) which is then applied proportionately to each zone. In other words, every zone (including the core) experiences a certain amount of blow-by proportional to its own mass. Although it is not physically realistic to model mass loss from zones that are not in contact with the ring pack, this approach was adopted in order to avoid inconsistent numerical solutions arising from the outermost zone reaching a zero-mass, zero-volume condition. Such a condition would result from the lack of inter-zonal mass transfer. Therefore, the blow-by model used herein represents a first attempt to incorporate the effects of cylinder mass loss in HCCI combustion and is not likely universally applicable.

3.4 Specification of model constants and initial conditions

Table 2 summarises the choice of initial conditions and model constants employed in all the multi-zone calculations. Below is a description of how these values have been estimated from or calibrated to measured experimental data.

Table 2 Multi-zone model constants and initial conditions

Intake pressure (Uniform)	0.97 bar
Residual gas fraction	10.9%
Average surface wall temperature	390 K
Intake temperature (core zone)	364 K
Blow-by rate constant (C_{BB})	5.5 s^{-1}
Core zone volume	10%
Geometric ratio (R)	1.0

3.4.1 Estimated model constants and initial conditions

Initially, each zone is assigned the same λ and EGR value. It is assumed that the entire intake charge is well mixed since EGR gases (CO_2, H_2O, N_2 and any excess O_2) are introduced to the intake manifold well upstream of the port and because fuel is injected directly onto the intake port itself. This procedure is analogous to the way in which a premixed SI engine charge is prepared.

The fraction of total charge mass associated with trapped residuals was estimated by considering the effective compression ratio or the cylinder volume ratio between exhaust valve closure (EVC = 15 deg ATDC) and IVC (34 deg ABDC). This ratio indicates a residual gas mass fraction of 10.9%. The effect of hot residual gas temperature has been absorbed into the specification of the intake temperature (discussed in Section 3.4.2) and the composition of residuals is assumed to be the same as EGR gas. Residual gases are also distributed evenly amongst all the zones since prior research (Babajimopoulos et al., 2003) has shown that excessively large amounts (usually associated with large negative

valve overlap) are required to affect in-cylinder composition distribution during the intake process.

A wall temperature of 390 K was specified for the model. Since this value is assigned to all in-cylinder surfaces and remains constant throughout the entire simulation, it is both a spatial and time averaged quantity. The wall temperature was estimated from the steady state coolant temperature of 369 K which was measured during engine operation. It is physically reasonable to use an average wall temperature that is higher than the steady coolant temperature since heat is lost to in-cylinder surfaces throughout the combustion process.

3.4.2 Calibrated model constants and initial conditions

Since HCCI is dominated by chemical kinetic processes, it tends to be very sensitive to initial conditions, especially intake temperature. Therefore, a calibration procedure was implemented in order to specify the remaining parameters in Table 2: intake temperature, blow-by constant, core zone volume and geometric ratio.

Two baseline operating points were considered in this process: Point A and Point B. These points are at $\lambda = 1.51$, EGR = 13.5% and $\lambda = 1.44$, EGR = 17.17%, respectively; their positions on the PRF20 engine operating map are indicated in Figure 1. Recall that all the other engine operating parameters were kept constant throughout the experimental work (Table 1). Both points are relatively close to the experimental knock boundary, but showed very stable combustion (i.e., the least amount of cyclic variability throughout the entire operating region). Calibration was carried out by specifying the remaining model parameters that provided the best pressure trace match to the experimental data at Point A. The specification of both estimated and calibrated model constants and initial conditions were then validated against Point B (Section 4.2). It is important to note that the experimental in-cylinder pressure trace data is an arithmetic average of 50 consecutive pressure signals.

The parameters adjusted during calibration were the intake temperature (T_{in}), the blow-by constant (C_{BB}), and the volume of the outermost zone which remains frozen at the wall temperature. Note that the outermost zone volume can be adjusted by varying the core zone volume and geometric ratio (R). The following procedure was employed in order to achieve an adequate pressure trace match to Point A:

1 Increase or decrease T_{in} in order to increase or decrease the peak pressure and advance or retard ignition timing.

2 Increase or decrease C_{BB} in order to match the pressure trace behaviour during the compression stroke.

3 Increase or decrease the volume of the outermost zone in order to increase or decrease peak pressure and match the pressure trace during the expansion stroke.

A calibrated intake temperature of 364 K is a reasonable value since it is close to the measured, regulated intake temperature of 361 K and because the charge likely gains heat from its interaction with hotter in-cylinder surfaces and residual gas. Note that the intake temperature is measured prior to the intake port and is not necessarily that of the charge at IVC (Atkins and Koch, 2005). The intake temperature is assigned only to the core zone. A linear temperature profile varying between T_{in} and the wall temperature of 390 K is then used as the initial temperature distribution among the zones at IVC.

The blow-by constant C_{BB} was calibrated to a value of 5.5 s^{-1}. This results in a loss of approximately 18% of the total mass which is initially trapped within the engine upon IVC. Although this value may seem unreasonably high, it should be noted that the engine operating speed was only 700 rpm and that previous work using a CFR engine has demonstrated mass losses between 20% and 30% (at 230 rpm) by Top Dead Center (TDC) (Fabbroni, 2004). At these low operating speeds there is more time for blow-by to occur in the engine. This speed effect is also compounded by the generally poor piston ring pack design associated with CFR engines. In the current model, blow-by is considered only up until the peak pressure is reached within the cylinder. Beyond this point, it is assumed that blow-by becomes negligible and significant mass loss does not occur. This assumption is based on several physical aspects of ring pack sealing. Firstly, after the main combustion event and throughout the rest of the expansion stroke, higher cylinder pressures help to force piston rings more snugly against cylinder walls and create a more effective seal. Secondly, due to the nature of splash lubrication (which is utilised in the CFR), there tends to be a completely flooded oil ring during the down-stroke of the piston (Ma et al., 1996). The accumulation of excess oil within the ring pack leads to more adequate sealing and a reduction in blow-by. Conversely, there tends to be lubrication starvation during the compression stroke where blow-by is most prevalent.

Previous work done by Eng et al. (1997) also indicates that blow-by ceases when the peak cylinder pressure is reached in a CFR engine. However, the same study predicted a total blow-by loss of only 8.8% at similar speed-load conditions. Furthermore, calculations using a simple, zero-dimensional ring-pack filling model demonstrated that 78% of the original charge mass forced into the ring pack returns to the cylinder by the time bottom dead centre is reached just after EVO. These findings highlight the simplicity of the blow-by model employed in the current work and emphasise that a more detailed investigation would require further refinement of the model to include universally applicable pressure, gas flow and ring pack geometry considerations.

The adjustment of T_{in} and C_{BB} allowed the model to be adequately calibrated in terms of ignition timing and pressure trace behaviour during the compression stroke. However, to accurately predict the peak pressure as well as the pressure trace behaviour during the expansion stroke, the amount of charge that remains frozen, non-reactive or unburned had to be adjusted. Incomplete combustion caused by bulk quenching near in-cylinder surfaces effectively inhibits the release of some chemical energy and leads to CO and UHC emissions. Prior research has shown that because HCCI engines typically operate at leaner conditions and achieve lower peak temperatures compared to SI engines, they exhibit substantial boundary layer and crevice volume quenching, as well as poor UHC oxidation prior to EVO (Milovanovic and Chen, 2001). The use of a chemically frozen wall zone in order to capture these effects is thus a realistic approach that has been previously employed in the multi-zone modelling literature (Komninos et al., 2004). In the current work, a physically non-reactive outermost zone was achieved by specifying a local heat transfer coefficient that would just maintain the zone at the wall temperature.

The outermost zone was calibrated to be 16.6% of the total initial cylinder volume at IVC. This value corresponds to an initial core zone volume of 10% and a geometric ratio of $R = 1$. When used with $T_{\text{in}} = 364$ K, $C_{BB} = 5.5$ s^{-1} and the other model parameters

summarised in Table 2, the pressure trace behaviour for Point A shown in Figure 4 was produced.

Figure 4 Multi-zone model prediction of pressure trace at Point A

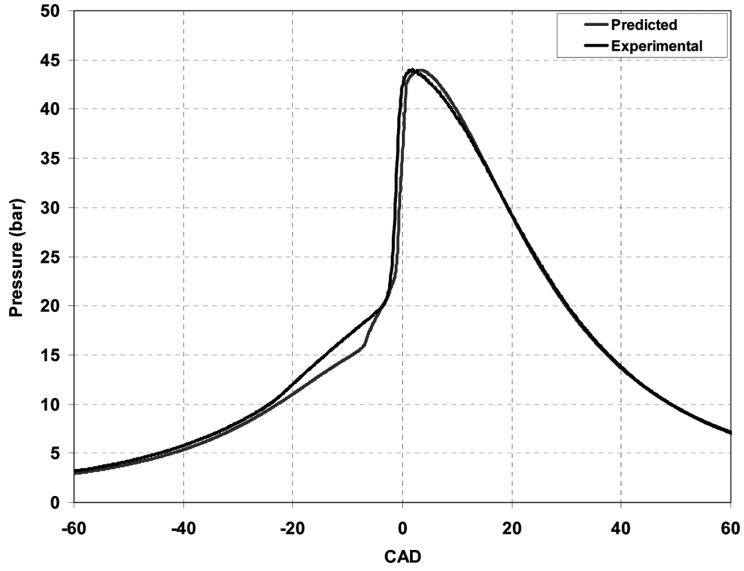

4 Results and discussion

4.1 Calibration analysis (Point A)

The prediction in Figure 4 shows good agreement in terms of second stage or main ignition timing as well as peak pressure. There is some discrepancy in terms of first stage ignition behaviour as the experimental data shows a very smooth cool flame region while the model predicts a shorter lived and more abrupt first stage ignition. PRF20 fuel is expected to exhibit significant first stage ignition behaviour and the discrepancy may be due to the inability of the reduced reaction mechanism to capture the chemical kinetic processes in this region. Regardless, it is the main or second stage combustion phenomenon that determines the prevalence of knock in the engine and this has been adequately reproduced.

Figure 5 shows a post simulation, single zone, adiabatic HRR analysis of the experimental and calculated pressure trace data for Point A. The HRR in J/CAD was calculated using the following equation with a constant $\gamma = 1.2$ and a central differencing scheme for derivatives:

$$\mathrm{HRR} = \left(\frac{1}{\gamma - 1}\right) V_{\mathrm{total}} \frac{\mathrm{d}P_{\mathrm{cyl}}}{\mathrm{d}\theta} + \left(\frac{\gamma}{\gamma - 1}\right) P_{\mathrm{cyl}} \frac{\mathrm{d}V_{\mathrm{total}}}{\mathrm{d}\theta}. \tag{16}$$

Although the model predicts a slightly delayed second-stage ignition for point A, this was the best timing that could be achieved with the calibration process employed. The inset to Figure 5 shows a more detailed view of what happens at about –20 CAD,

demonstrating that there is indeed some experimental heat release due to low-temperature kinetics. In every region other than that identified by the inset, the HRR maintains a near zero average – only at around –20 CAD does the curve deviate from this average, indicating the presence of chemical heat release. The multi-zone model predicts the onset of cool flame ignition at around –7 CAD. As previously mentioned, this is most likely due to the misrepresentation of low temperature kinetics in the reduced PRF chemical mechanism. The need to curtail this energy release which occurs so close to top dead centre helps to explain the relatively high calibration value for blow-by loss (~18%). Finally, it is important to note that the 'jagged' nature of the predicted HRR is an inherent feature of multi-zone models (a detailed treatment of which is given in Section 4.3.1).

In order to verify that the calibration procedure yielded a physically reasonable amount of frozen charge mass, a comparison between the predicted and measured emissions was carried out. At operating Point A, the engine produced 7.9 g/kWhr of CO and 29.8 g/kWhr of UHC for an indicated specific fuel consumption of 285 g/kWhr. This means that a combined amount of 0.132 g of CO and UHC was produced per gram of fuel consumed. Analysis of the exhaust composition predicted by the model at the end of the closed cycle indicated a value of $(m_{CO} + m_{UHC})/m_{FUEL} = 0.133$, which closely matches the measured quantity. This value was obtained by summing all of the UHC species and CO over every zone just prior to EVO and dividing by the total calculated mass of fuel introduced. The results are summarised in Table 3.

Figure 5 Heat Release Rate analysis at Point A (Inset: detail of region between –25 CAD and –10 CAD)

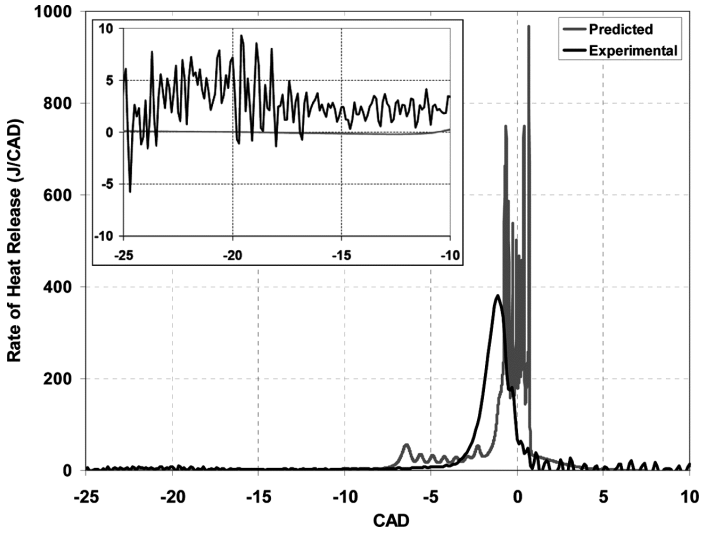

Table 3 Relative CO and UHC emissions for Point A and Point B

		$(m_{CO} + m_{UHC})/m_{FUEL}$
Point A	Measured	0.132
	Predicted	0.133
Point B	Measured	0.121
	Predicted	0.133

4.2 Model validation (Point B)

In order to determine whether or not the calibration of initial conditions and model constants presented above is in fact robust, the model was used to reproduce the pressure trace at Point B as well. This procedure required nothing more than changing the operating point parameters to $\lambda = 1.44$ and EGR = 17.17%. All other modelling and engine parameters were kept the same. The results are summarised in Figures 6 and 7 and Table 3.

Figure 6 Multi-zone model prediction of pressure trace at Point B

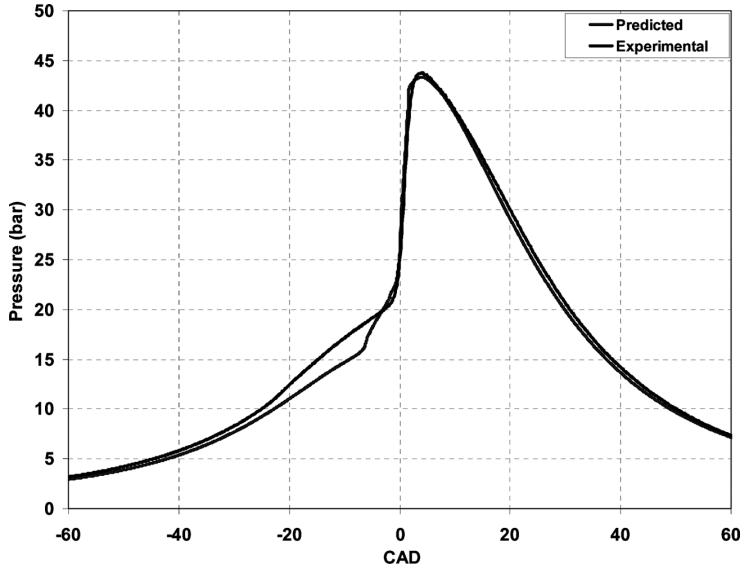

Figure 7 Heat Release Rate analysis at Point B (Inset: detail of region between –25 CAD and –10 CAD)

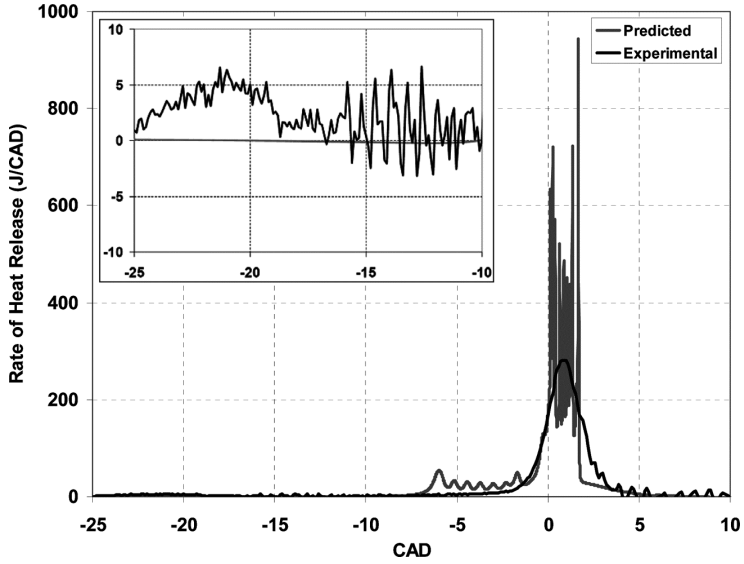

The calibration performed at Point A shows very good transference to Point B: both second stage ignition timing and peak pressure behaviour were accurately predicted without any adjustments to model parameters. The same type of discrepancy in cool flame activity is also exhibited, but the HRR analysis indicates excellent agreement with respect to second stage ignition timing. The inset to Figure 7 also shows a clear distinction between the experimental low-temperature HRR and the otherwise zero-average chemical energy release along the compression stroke. The emission result in Table 3 does not show much change in the predicted value, although it still lies within 10% of the measured emissions. This is considered as good agreement given the various assumptions associated with in-cylinder conditions. These results indicate that the multi-zone model is fairly robust with respect to the current experimental data set. With this validation in place, it is possible to attempt to predict the knock boundary for the engine corresponding to PRF20.

4.3 Knock boundary prediction

Two different techniques were used to reproduce the experimental HCCI engine knock boundary. The first method relies on MPRR while the second is based on the β_k parameter developed by Yelvington and Green (2003). Each method is treated separately here and then compared.

4.3.1 Knock boundary prediction using MPRR

One major disadvantage associated with using MPRR to predict the knock boundary is that it requires calibration. In other words, the experimental knock boundary is required in order to determine the MPRR that corresponds to engine knock under the given operating conditions. Afterwards, this criterion can be used to try and reproduce the rest of the knock boundary. Since all of the engine operating parameters were kept constant during the experimental study (see Table 1), the onset of knock should only be a function of dilution within the charge. In order to find the MPRR that corresponds to the experimental knock boundary, a λ dilution path passing through Point A was chosen. The EGR rate was fixed to 13.57% (Point A) and λ was varied between 1.42 and 1.72. This dilution path ranges from within the centre of the PRF20 operating range to beyond the experimental knock boundary. The multi-zone model was used to generate pressure traces for various points along this dilution path. The pressure rise rate was calculated from the predicted pressure profiles using a central differencing scheme.

The MPRR in terms of bar/CAD was extracted from the modelled data. Calculated rates of change have a strong dependency on the size of the time step or crank angle step that is chosen. Therefore, the variation of $\mathrm{d}P/\mathrm{d}\theta|_{max}$ (or MPRR) to time step size was investigated at several operating points and shown to be insensitive for a $\Delta t \leq 10^{-6}$ s. As a result, a time step size of 10^{-6} s was used for all subsequent simulations. Table 4 shows the typical behaviour that was observed. The MPRR results for the dilution path passing through Point A are shown in Figure 8. One interesting result here is that the MPRR varies linearly with excess air dilution. This linear behaviour persists in the calculations just beyond the experimental knock boundary where the pressure equalisation process and thus the multi-zone model assumptions become invalid. Figure 8 also shows similar results for an excess air dilution path that passes

through Point B. Both lines indicate that the experimental knock boundary corresponds to a MPRR of approximately 39 bar/CAD.

Figure 8 Predicted MPRR vs. λ for an excess air dilution path through Point A (EGR = 13.57%) and Point B (EGR = 17.17%)

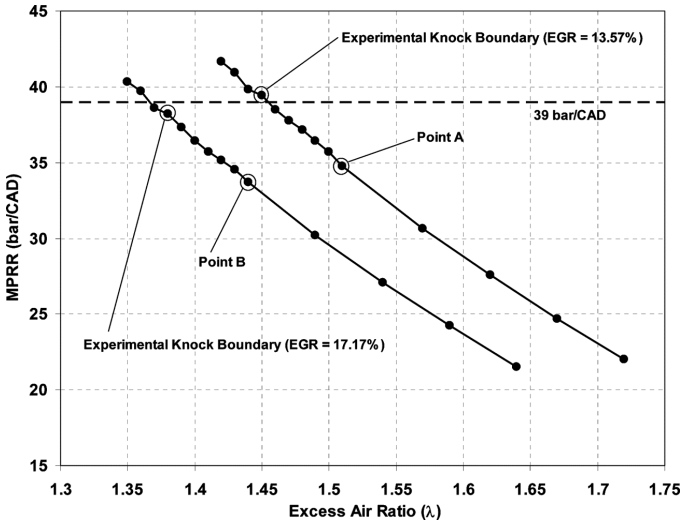

Table 4 Sensitivity of MPRR to time step size Δt (at Point A)

Time step size, Δt (s)	$dP/d\theta\,|_{max}$ (bar/CAD)
10^{-5}	19.25
10^{-6}	34.72
10^{-7}	34.84

In the work by Yoshizawa et al. (2006), Kalghatgi and Head (2005) and Yao et al. (2007), a MPRR criterion of 3–10 bar/CAD was used in order to define the knock boundaries for typical HCCI engine operating speeds between 1200 rpm and 3000 rpm. Direct analysis of the experimental pressure traces for points A and B reveal MPRRs of only 13.6 and 9.9 bar/CAD, respectively. Both of these points are near the measured high load limit and exhibit MPRRs that are comparable to those in previous studies. Therefore, it seems unreasonable to have adopted a knock limit criterion almost four times higher. The much higher MPRR criterion encountered herein is a consequence of the 'jagged' heat release behaviour inherent to multi-zone models. This jagged nature arises from the fact that zones ignite discretely in time as homogeneous mixtures. When these perfectly mixed reactors release their chemical energy over a very short time scale, a spike in HRR is observed. It is clear from Figures 5 and 7 that the pressure rise rates associated with individual zone ignitions exceed the global pressure rise rate calculated from the experimental data. This is why the predicted MPRR for points A and B were 34.7 and 33.7 bar/CAD, respectively, and why a value of 39 bar/CAD was needed to calibrate the MPRR criterion for subsequent calculations. An attempt was made in order to smooth out the predicted HRR by fitting cubic splines to the original pressure trace calculations. However, this method did not produce an adequate prediction of the experimental

knock boundary. An additional investigation into pressure trace smoothing through the use of higher zone numbers was simply not feasible for the current work because of the associated cost of computational time.

The MPRR knock criterion of 39 bar/CAD was therefore tested to see how well it could reproduce the experimental high load limit. A simple method using linear interpolation was employed since the MPRR vs. excess air dilution trends themselves were found to be linear. Two operating points (one within the operating region and one outside it) that bracket the experimental knock boundary and are equidistant in terms of excess air dilution were chosen at various EGR rates. Pressure traces were generated for all these points along with their corresponding MPRRs. At a given EGR rate, the λ at which knock is expected is calculated via interpolation of the MPRRs to 39 bar/CAD. The calculated knock boundary is plotted in Figure 9. The prediction is quite adequate for every point but the last. This may be due to the use of EGR rate in the interpolation as opposed to excess air. Only the last point in the MPRR trend was interpolated using EGR instead of excess air rates so that an excess air ratio of unity would not be exceeded in the simulations. Since the linearity of MPRR vs. EGR dilution rate was never confirmed, this last point may not be as reliable as the other points on the predicted knock boundary.

Regardless of the discrepancy in the last point, the results in Figure 9 indicate that MPRR is a valid criterion for describing the knock limit of HCCI engines. Furthermore, adopting an MPRR knock criterion which is higher than the experimentally observed global pressure rise rate did not affect the quality of the high load limit prediction.

Figure 9 Comparison of predicted knock boundaries using the MPRR and β_k criteria

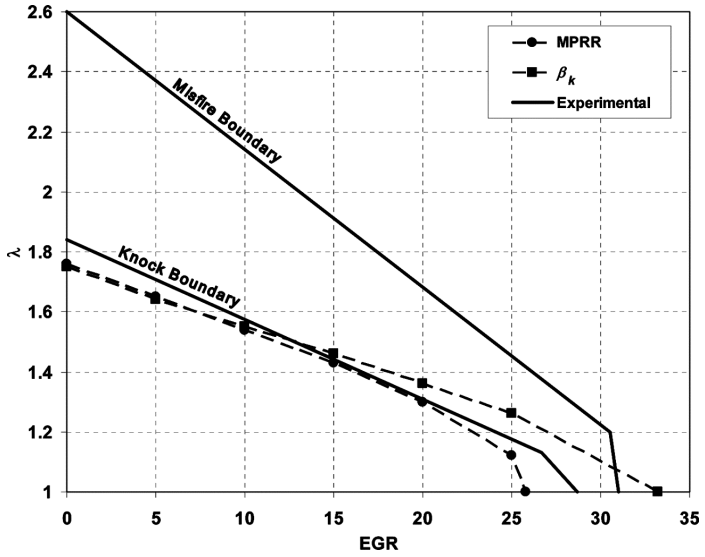

4.3.2 Knock boundary prediction using β_k

The dimensionless parameter β_k (equation (1)) can be used to evaluate the tendency of HCCI engines to experience knock. Analogous to the work done in Yelvington et al. (2004), the pressure term P was simply taken from the predicted pressure trace data. Note that the knock factor may be calculated during the combustion simulation since

the instantaneous HRR, cylinder pressure and ratio of specific heats are updated at every time step. However, Yelvington and Green (2003) and Yelvington et al. (2004) determine β_k post-simulation, and the same approach was used here for consistency. Calculation of the remaining parameters in equation (1) is described below.

Recall that L_c is a characteristic length scale for the problem. In Yelvington and Green (2003), the authors assigned 1/10th of the cylinder bore diameter to L_c for their multi-zone calculations and stated that it represented the scale of homogeneities within the charge. Even when using a single-zone model in Yelvington et al. (2004) the same approach was adopted. In this study, a value of L_c equal to the total bore diameter was found to provide adequate results despite the presence of ten zones which are stratified in temperature. This verifies that L_c is a description of species homogeneity and that the engine charges that were modelled in Yelvington and Green (2003) were less homogeneous than the ones considered here.

The ratio of specific heats (γ) is a function of species concentration and temperature but was assigned an average value of 1.2 to be consistent with the approach used in Yelvington and Green (2003) and Yelvington et al. (2004). The rate of chemical heat release per unit volume ($\dot{q}$) was calculated by multiplying the molar rate of change of all fuel components by their corresponding heats of combustion:

$$\dot{q} = \frac{\left(\frac{\mathrm{d}N_{\mathrm{oct}}}{\mathrm{d}t} \cdot h_{\mathrm{oct}} + \frac{\mathrm{d}N_{\mathrm{hep}}}{\mathrm{d}t} \cdot h_{\mathrm{hep}} \right)}{V}. \tag{17}$$

The molar rates of change were calculated using a central differencing scheme in order to be consistent with the determination of MPRR. Any contribution in the change in moles due to blow-by was negated by using the rate of change of fuel mole fraction and multiplying by total moles of the previous time step:

$$\left. \frac{\mathrm{d}N_{\mathrm{fuel}}}{\mathrm{d}t} \right|_t = N_{\mathrm{total}}\big|_{t-\Delta t} \cdot \left. \frac{\mathrm{d}X_{\mathrm{fuel}}}{\mathrm{d}t} \right|_t. \tag{18}$$

It is assumed here that since the points being considered are near the knock limit, combustion efficiency should be high and most of the fuel's energy would be completely released into the charge.

The speed of sound was calculated with the following relation:

$$u_{\mathrm{sound}} = \sqrt{\gamma R_{\mathrm{mix}} T}. \tag{19}$$

The same points that were used to bracket the experimental knock boundary in the determination of MPRR were processed to calculate β_k. A value of β_k was generated at every instant and for every zone. From this data, a maximum value of β_k was extracted and a λ value for each EGR rate which corresponds to $\beta_k = 1$ was interpolated (analogous to the MPRR criterion). As before, simulations were carried out for values of $\beta_k > 1$ where it is known that the multi-zone model assumptions break down. However, the linearity of MPRR vs. excess air ratio beyond the knock boundary (see Figure 8) suggests that this interpolative approach is still valid since both criteria are related to one another via the global pressure rise rate in the charge (Yelvington and Green, 2003). The predicted knock boundary using β_k is shown in Figure 9.

Despite being fundamentally related, the MPRR and β_k criteria show some discrepancy in their prediction of the knock boundary. The greatest deviation occurs for large EGR rates and low excess air ratios. A possible explanation for these discrepancies may be attributed to in-cylinder mixture quality effects. Fuel, air and EGR gases are introduced to the engine well upstream of the intake port. However, engine speed is low and some small partially mixed pockets of gas are likely to develop within the charge. This would be especially true at higher EGR rates where the greatest deviation between predicted knock boundaries occurs. The existence of small regions of slightly richer and higher temperature mixture does not drastically affect the phasing or duration of HCCI combustion (Richter et al., 2000; Girard et al., 2002; Thirouard et al., 2005). This is because ignition occurs in these regions simultaneously at several different locations, essentially dampening out the effect of non-uniformities (in other words, when β_k remains less than 1). However, the length scale of homogeneity is an input to the β_k criterion via L_c. It is likely that as the EGR rate increases, the charge is less homogeneous and L_c is reduced (when L_c is equal to the bore diameter, it indicates that the charge is completely mixed, anything less means there are variations in mixture homogeneity within the charge). For a fixed HRR, this would shift the β_k predicted knock boundary downwards in Figure 9, closer to the MPRR calculation and the experimental high load limit. Physically, this shift in the boundary means that a smaller volume of gas needs to expand and therefore the propensity to knock at lower excess air dilution rates is reduced.

Another possible explanation for the discrepancy between the models is the use of a constant ratio of specific heats. In reality, γ varies with mixture composition and temperature throughout the combustion process. Figure 9 indicates that at lower EGR rates, assuming $\gamma = 1.2$ does not affect the quality of the knock limit prediction. However, this assumption tends to break down at higher EGR dilution rates. Once again, it should be noted that the last point in the β_k criterion knock boundary was generated using interpolation of EGR dilution rates.

These results indicate that both the MPRR and β_k criterion are able to capture the experimental knock boundary with reasonable accuracy. Although the MPRR criterion more adequately describes the high load limit, the β_k criterion has an advantage in that it does not require a specific calibration process (apart from specifying an appropriate value for L_c) in order to predict the knock boundary for HCCI engines.

5 Conclusions

A multi-zone methodology was developed in order to predict the combustion behaviour of an experimental HCCI engine using PRF20. A simple blow-by model was introduced in order to more accurately capture the operation of the engine which runs at a relatively low speed of 700 rpm. The multi-zone model was calibrated by matching its predictions to the observed in-cylinder pressure trace at a single operating point (Point A). The model's robustness was validated by using it to reproduce the pressure trace of another engine operating point (Point B) without any further parameter adjustments. The experimental and predicted relative emissions of CO and UHC were also compared showing good agreement and further verifying the model's robustness.

The experimental knock boundary of the HCCI engine was also reproduced using two different predictive criteria. The first is based on the MPRR in the engine and the second is based on the dimensionless β_k factor. Preliminary testing of the MPRR criterion revealed that it varies linearly with excess air dilution. The interpolated knock boundary predictions based on these two separate criteria showed good agreement with experimental results. Up to an EGR rate of about 15% the two predicted knock boundaries are essentially identical after which they begin to diverge substantially. It is the MPRR criterion that captures the experimental knock boundary more accurately at higher EGR rates. However, the β_k criterion has an advantage in that it does not require a specific calibration process (apart from specifying an appropriate value for L_c) in order to predict the knock boundary as does the MPRR criterion.

In general, the results of this work have demonstrated that a stand alone multi-zone model devoid of detailed CFD calculations can be used to adequately reproduce the knock boundary of HCCI engines.

Acknowledgements

The authors would like to graciously thank Auto 21 Networks of Centers of Excellence, the Ontario Graduate Scholarship Program and the Natural Sciences and Engineering Research Council of Canada for their financial support of this project. Other individuals who merit a special thanks for their contributions include Professor J.S. Wallace (University of Toronto) and M. Shahbakhti (University of Alberta).

References

Aceves, S.M., Martinez-Frias, J., Flowers, D.L., Smith, J.R., Dibble, R.W., Wright, J.F. and Hessel, R.P. (2001) *A Decoupled Model of Detailed Fluid Mechanics Followed by Detailed Chemical Kinetics for Prediction of Iso-Octane HCCI Combustion*, SAE Technical Paper No. 2001-01-3612, pp.1–12.

Atkins, M.J. and Koch, C.R. (2005) 'The effect of fuel octane and dilutent on homogeneous charge compression ignition combustion', *Proceedings of the Institution of Mechanical Engineers, Part D – Journal of Automobile Engineering*, Vol. 219, pp.665–675.

Babajimopoulos, A., Lavoie, G.A. and Assanis, D.N. (2003) *Modeling HCCI Combustion with High Levels of Residual Gas Fraction – A Comparison of Two VVA Strategies*, SAE Technical Paper No. 2003-01-3220.

Babajimopoulos, A., Assanis, D.N., Flowers, D.L., Aceves, S.M. and Hessel, R.P. (2005) 'A fully coupled computational fluid dynamics and multi-zone model with detailed chemical kinetics for the simulation of premixed charge compression ignition engines', *International Journal of Engine Research*, Vol. 6, pp.497–512.

Chang, J., Gurlap, O., Filipi, Z., Assanis, D., Kuo, T., Najt, P. and Rask, R. (2004) *New Heat Transfer Correlation for an HCCI Engine Derived from Measurements of Instantaneous Surface Heat Flux*, SAE Technical Paper No. 2004-01-2996, pp.1–18.

Cheng, K.Y., Shayler, P.J. and Murphy, M. (2004) 'The influence of blow-by on indicated work output from a diesel engine under cold start conditions', *Proceedings of the Institution of Mechanical Engineers: Part D – Journal of Automobile Engineering*, Vol. 218, pp.333–340.

Christensen, M. and Johansson, B. (2002) *The Effect of In-Cylinder Flow and Turbulence on HCCI Operation*, SAE Technical Paper No. 2002-01-2864, pp.1–12.

Christensen, M., Johansson, B. and Einewall, P. (1997) *Homogeneous Charge Compression Ignition (HCCI) Using Isooctane, Ethanol and Natural Gas – A Comparison with Spark Ignition Operation*, SAE Technical Paper No. 972874, pp.1–11.

Eng, J.A., Leppard, W.R., Najt, P.M. and Dryer, F.L. (1997) *Experimental Hydrocarbon Consumption Rate Correlations from a Spark Ignition Engine*, SAE Technical Paper No. 972888, pp.41–62.

Fabbroni, M.A. (2004) *Flame Propagation in Natural Gas Fuelled Direct Injection Engines*, Master's Thesis, University of Toronto, Toronto, Ontario, Canada.

Ferguson, C.R. (1986) *Internal Combustion Engines*, John Wiley & Sons, Toronto.

Flowers, D., Aceves, S., Smith, R., Torres, J., Girard, J. and Dibble R. (2000) *HCCI in a CFR Engine: Experiments and Detailed Kinetic Modeling*, SAE Technical Paper No. 2000-01-0328, pp.13–26.

Girard, J.W., Dibble, R.W., Flowers, D.L. and Aceves, S.M. (2002) *An Investigation of the Effect of Fuel-Air Mixedness on the Emission from an HCCI Engine*, SAE Technical Paper No: 2002-01-1758, pp.1–8.

Griffiths, J.F., MacNamara, J.P., Sheppard, C.G.W., Turton, D.A. and Whitaker, B.J. (2002) 'The relationship of knock during controlled autoignition to temperature inhomogeneities and fuel reactivity', *Fuel*, Vol. 81, pp.2219–2225.

Heywood, J.B. (1988) *Internal Combustion Engine Fundamentals*, McGraw-Hill, Toronto.

Kalghatgi, G.T. and Head, R.A. (2005) 'Combustion limits and efficiency in a homogeneous charge compression ignition engine', *International Journal of Engine Research*, Vol. 7, pp.215–235.

Kee, R.J., Rupley, F.M., Miller, J.A., Coltrin, M.E., Grcar, J.F., Meeks, E., Moffat, H.K., Lutz, A.E., Dixon-Lewis, G., Smooke, M.D., Warnatz, J., Evans, G.H., Larson, R.S., Mitchell, R.E., Petzold, L.R., Reynolds, W.C., Caracotios, M., Stewart, W.E., Glarborg, P., Wang, C. and Adigun, O. (2000) *CHEMKIN Collection*, Release 3.6, Reaction Design Inc., San Diego, CA.

Kee, R.J., Rupley, F.M., Miller, J.A., Coltrin, M.E., Grcar, J.F., Meeks, E., Moffat, H.K., Lutz, A.E., Dixon-Lewis, G., Smooke, M.D., Warnatz, J., Evans, G.H., Larson, R.S., Mitchell, R.E., Petzold, L.R., Reynolds, W.C., Caracotios, M., Stewart, W.E., Glarborg, P., Wang, C., Adigun, O., Houf, W.G., Chou, C.P. and Miller, S.F. (2003) *CHEMKIN Collection*, Release 3.7.1, Reaction Design Inc., San Diego, CA.

Komninos, N.P., Hountalas, D.T. and Kouremenos, D.A. (2004) *Development of a New Multi-Zone Model for the Description of Physical Processes in HCCI Engines*, SAE Technical Paper No. 2004-01-0562.

Ma, M-T., Sherrington, I. and Smith, E.H. (1996) 'Implementation of an algorithm to model the starved lubrication of a piston ring in distorted bores: prediction of oil flow and onset of gas blow-by', *Proceedings of the Institution of Mechanical Engineers: Part J – Journal of Engineering Tribology*, Vol. 210, pp.29–44.

Milovanovic, N. and Chen, R. (2001) *A Review of Experimental and Simulation Studies on Controlled Auto-Ignition Combustion*, SAE Technical Paper No. 2001-01-1890, pp.1–10.

Oakley, A., Zhao, H., Ladommatos, N. and Ma, T. (2001a) *Dilution Effects on the Controlled Auto-Ignition (CAI) Combustion of Hydrocarbon and Alcohol Fuels*, SAE Technical Paper No. 2001-01-3606, pp.1–14.

Oakley, A., Zhao, H., Ladommatos, N. and Ma, T. (2001b) *Experimental Studies on Controlled Auto-Ignition (CAI) Combustion of Gasoline in a 4-Stroke Engine*, SAE Technical Paper No. 2001-01-1030, pp.1–14.

Onishi, S., Jo, S.H., Shoda, K., Jo, P.D. and Kato, S. (1979) *Active Thermo-Atmosphere Combustion (ATAC) – A New Combustion Process for Internal Combustion Engines*, SAE Technical Paper No. 790501, pp.1–10.

Richter, M., Engstrom, J., Franke, A., Alden, M., Hultqvist., A. and Johansson, B. (2000) *The Influence of Charge Inhomogeneity on the HCCI Combustion Process*, SAE Technical Paper No. 2000-01-2868.

Suzuki, H., Koike, N., Ishi, H. and Odaka, M. (1997) *Exhaust Purification of Diesel Engines by Homogeneous Charge with Compression Ignition Part 1: Experimental Investigation of Combustion and Exhaust Emission Behavior Under Pre-Mixed Homogeneous Charge Compression Ignition Method*, SAE Technical Paper No. 970313, pp.1–9.

Tanaka, S., Ayala, F. and Keck, J.C. (2003) 'A reduced chemical kinetic model for HCCI combustion of primary reference fuels in a rapid compression machine', *Combustion and Flame*, Vol. 133, pp.467–481.

Thirouard, B., Cherel, J. and Knop, V. (2005) *Investigation of Mixture Quality Effect on CAI Combustion*, SAE Technical Paper No. 2005-01-0141.

Thring, R.H. (1989) *Homogeneous-Charge Compression-Ignition (HCCI) Engines*, SAE Technical Paper No. 892068, pp.1–9.

Tzanetakis, T. (2006) *Multi-Zone Modelling of a Primary Reference Fuel HCCI Engine*, Master's Thesis, University of Toronto, Toronto, Ontario, Canada.

Yao, M., Zhang, B., Zheng, Z., Chen, Z. and Xing, Y. (2007) 'Effects of exhaust gas recirculation on combustion and emissions of a homogeneous charge compression ignition engine fuelled with primary reference fuels', *Proceedings of the Institution of Mechanical Engineers: Part D – Journal of Automobile Engineering*, Vol. 221, pp.197–213.

Yelvington, P.E., and Green, W.H. (2003) *Prediction of the Knock Limit and Viable Operating Range for a Homogeneous-Charge Compression-Ignition (HCCI) Engine*, SAE Technical Paper No. 2003-01-1092, pp.1–8.

Yelvington, P.E., Rallo, M.I., Liput, S., Tester, J.W., Green, W.H. and Yang, J. (2004) 'Prediction of performance maps for homogeneous charge compression ignition engines', *Combustion Science and Technology*, Vol. 176, pp.1243–1282.

Yoshizawa, K., Teraji, A., Miyakubo, H., Yamaguchi, K. and Urushihara, T. (2006) 'Study of high load operation limit expansion for gasoline compression ignition engines', *Journal of Engineering for Gas Turbines and Power*, Vol. 128, pp.377–387.

Nomenclature

C_{BB}	Blow-by constant
c_p	Specific heat at constant pressure
CR	Compression ratio
c_v	Specific heat at constant volume
h_x	Heat of combustion for species 'x'
K	Number of species in chemical kinetic reaction mechanism
L_c	Characteristic length scale of inhomogeneities
M	Mass
$\dot{m}_{BB}$	Blow-by rate
m_{out}	Mass lost due to blow-by
MW	Molecular weight
N_x	Moles of species 'x'
N_{total}	Total moles in mixture
P	Pressure

P_{cyl}	Equalised cylinder pressure
$\dot{q}$	Chemical rate of heat release per unit volume
R	Geometric zone ratio
R_i	Gas constant (for zone i)
R_{mix}	Gas constant (for mixture)
R_l	Ratio of connecting rod length to crank arm radius
R_u	Universal gas constant
T	Temperature
t	Time
T_{in}	Intake temperature (applied to core zone)
u	Specific internal energy
u_{sound}	Speed of sound
V	Zone volume
V_c	Cylinder clearance volume
V_{total}	Total instantaneous cylinder volume
Y	Species mass fraction
X_{fuel}	Mole fraction of fuel
β_k	Dimensionless knock parameter (see equation (1))
β	Blow-by parameter (see equation (14))
γ	Ratio of specific heats (c_p/c_v)
θ	Crankshaft rotation angle
λ	Actual air-fuel ratio divided by stoichiometric air-fuel ratio (excess air ratio)
ρ	Density
ω	Engine speed
$\dot{\omega}$	Molar species formation rate

Acronyms

ABDC	After Bottom Dead Center
ATDC	After Top Dead Center
BBDC	Before Bottom Dead Center
BTDC	Before Top Dead Center
CAD	Crank Angle Degrees
CFD	Computational Fluid Dynamics
CFR	Cooperative Fuels Research
CI	Compression Ignition
CO	Carbon monoxide
CO_2	Carbon dioxide
EGO	Exhaust Gas Oxygen

EGR	Exhaust Gas Recirculation
EVC	Exhaust Valve Closure
EVO	Exhaust Valve Open
HCCI	Homogeneous Charge Compression Ignition
HRR	Heat Release Rate
H_2O	Water
IMEP	Indicated Mean Effective Pressure
IVC	Intake Valve Closing
MPRR	Maximum Pressure Rise Rate
NO_x	Nitrogen oxides
N_2	Nitrogen gas
O_2	Oxygen gas
PRF	Primary Reference Fuel
RCM	Rapid Compression Machine
SI	Spark Ignition
TDC	Top Dead Centre
UHC	Unburned Hydrocarbons